# Strong charge-carrier localization in InAs/GaAs submonolayer stacks prepared by Sb-assisted metalorganic vapor-phase epitaxy

D. Quandt,* J.-H. Schulze, A. Schliwa, Z. Diemer, C. Prohl, A. Lenz, H. Eisele, A. Strittmatter, U. W. Pohl, M. Gschrey, S. Rodt, S. Reitzenstein, and D. Bimberg
*Institut für Festkörperphysik, Technische Universität Berlin, Hardenbergstrasse 36, D-10623 Berlin, Germany*

M. Lehmann
*Institut für Optik und Atomare Physik, Technische Universität Berlin, Strasse des 17. Juni 135, D-10623 Berlin, Germany*

M. Weyland
*Monash Centre for Electron Microscopy & Department of Materials Engineering, Monash University, VIC 3800, Australia*
(Received 27 February 2015; revised manuscript received 21 May 2015; published 15 June 2015)

Stacks of InAs/GaAs submonolayer depositions forming small In-rich islands are interesting for efficient optoelectronic applications due to the high areal density of localization centers and their fast carrier relaxation. The electronic confinement of charge carriers in InAs/GaAs submonolayers can be influenced by adding Sb during growth. Eight-band $k \cdot p$ simulations show that electrons and holes experience a different localization depending on where the Sb is incorporated into the submonolayer stacks. Samples grown with metalorganic vapor-phase epitaxy show sharp interfaces between InAs(Sb)/GaAs submonolayers and the surrounding matrix material in transmission electron microscopy and x-ray diffraction measurements. Cross-sectional scanning tunneling microscopy shows the formation of In-rich agglomerations as well as a slight clustering of Sb atoms. Temperature-dependent photoluminescence and spatially resolved cathodoluminescence show evidence for strong electronic confinement whose depth is controlled by the Sb amount.

DOI: 10.1103/PhysRevB.91.235418 PACS number(s): 81.07.Ta, 81.15.Kk, 81.05.Ea

## I. INTRODUCTION

Modern semiconductor-based coherent light sources employ as an active region either quantum well (QW) layers or quantum dot (QD) ensembles, exhibiting two-dimensional (2D) or zero-dimensional (0D) localization of charge carriers, respectively. Owing to their three-dimensional (3D) confinement potential, QDs offer higher material gain and better temperature stability than QWs [1–3]. Epitaxial QDs evolving from Stranski-Krastanov growth of a strained InAs/GaAs layer have maximal areal densities limited to about $10^{10}$–$10^{11}$ cm$^{-2}$ due to their typical base lengths of 7–26 nm [3–10]. Recently we have proven high densities of closely neighbored In-rich agglomerations ($10^{12}$ cm$^{-2}$) occurring within InAs/GaAs submonolayer (SML) stacks grown by metalorganic vapor phase epitaxy (MOVPE) [11,12]. The deposition of 1 SML of strained material leads to high densities of small islands with up to 8 monolayers (MLs) height [11], which are subsequently buried by matrix material with a higher band gap. Stacks of submonolayers can be realized by cycled deposition of a SML and a few MLs of barrier material, which results in high-density ensembles of localization centers without employing a strain-driven 2D/3D growth-mode transition [13]. Structural coupling along the growth direction of such SML islands is mediated by strain fields originating from each island towards the growth front [14]. Samples grown by molecular beam epitaxy show a density of about $5 \times 10^{11}$ cm$^{-2}$, acting as 0D localization centers as found by microphotoluminescence (PL) [15–17]. Samples grown using MOVPE exhibit photoluminescence properties, which are best described as a mixture of QD-like 0D and quantum-well-like 2D states. This is likely attributed to strong lateral electronic coupling induced by laterally closely spaced In-rich agglomerations [12].

The high density and uniformity of the In-rich islands leads to a high gain of the SMLs as active material [18] and enables the fabrication of devices with lower internal losses and higher differential gain as compared to Stranski-Krastanov QDs [19]. The increased differential gain allows for higher modulation bandwidths [20,21]. High power diode lasers [22], semiconductor disk lasers [23], and VCSELs [24,25] were successfully demonstrated.

Additionally it has been shown that the coupling of SMLs via stacking allows for tuning of the polarization properties [26,27].

In this work we theoretically and experimentally investigate the influence of Sb as an additional atomic species on the electronic and optical properties of InAs/GaAs submonolayer stacks. Eight-band $k \cdot p$ simulations [28] determine the influence of Sb on the wave functions of electrons and holes for different incorporation schemes. The structural and optical properties of InAs(Sb)/GaAs-SML stacks are investigated using x-ray diffraction (XRD), scanning transmission electron microscopy (STEM), cross-section scanning tunneling microscopy (XSTM), temperature-dependent photoluminescence, and spatially resolved cathodoluminescence (CL). Sb incorporation into the In-rich regions formed by submonolayer growth is determined. The In-rich regions in the SML stacks are referred to as QDs in the following. The Sb incorporation into the QDs results in an enhanced localization of the hole wave function, and an increasing full width at half maximum (FWHM) of the PL intensity.

*dquandt@physik.tu-berlin.de

 ©2015 American Physical Society

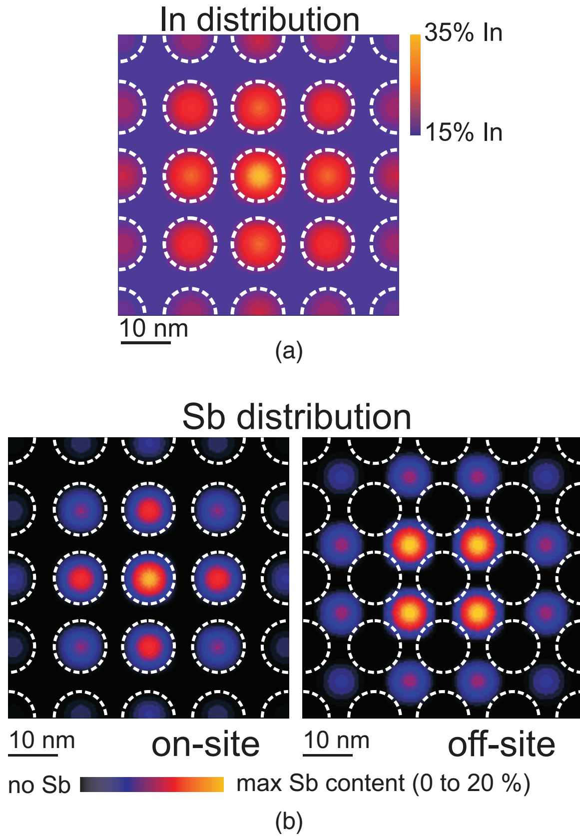


FIG. 1. (Color online) In and Sb distributions assumed for the eight-band $k \cdot p$ simulations, the dashed white circles indicate the positions of the QDs as defined by In-rich regions: (a) In distribution, the maximum local In content is 35%, a sigmoidal In distribution is used. (b) Sb distributions for the cases (a) and (c), the maximum local Sb content is 20%.

## II. SIMULATION

Eight-band $k \cdot p$ simulations show that electrons and holes react differently to the presence of Sb in an InAs/GaAs submonolayer stack. The basic structure for the simulation consists of an 8.5-nm-thick InGaAs quantum well with 15% In content. Spherical In-rich agglomerations with a sinusoidal composition profile, a maximum local In content of 35%, and a spacing of 13.6 nm are embedded into this quantum well [see Fig. 1(a)].

For the distribution of the antimony, three cases are considered:

(a) The Sb is incorporated into the QDs [Fig. 1(b) left].

(b) Even distribution of the Sb throughout the SML stack (not shown).

(c) Incorporation of Sb in between the QDs [Fig. 1(b) right].

The maximum Sb content was varied from 0 to 20%. The incorporation of Sb into the SML stack leads to a redshift of the PL emission in all three simulated cases (see Fig. 2). The strongest shift is found for case (b) where an homogenous incorporation of 10% Sb leads to a redshift of about 140 meV. To achieve a similar redshift for the two other cases, a peak Sb content of more than 20% is necessary. Electron and hole wave

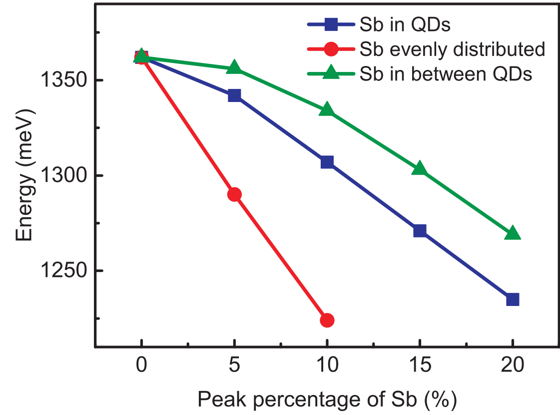


FIG. 2. (Color online) Simulated PL emission energies dependent on the maximum local Sb content for the three different distributions.

functions react quite differently to Sb incorporation. Holes localize at the Sb-rich regions (see Fig. 6), while the electrons localize at the In-rich regions and delocalize from Sb-rich regions (see Fig. 4).

The spatial distribution of the wave functions influences the electric dipole moment in the semiconductor structure. Their overlap defines the Huang-Rhys factor [29], which is also a measure for coupling to LO phonons. A better overlap of the wave functions leads to a smaller Huang-Rhys factor. Figure 3 shows the band structure for the three different assumptions on Sb incorporation together with the case without Sb.

In case (a), the Sb incorporated into the QDs leads to a stronger localization of the hole wave function, whereas the electron wave function delocalizes (Figs. 3 and 4). This results in a reduced electron-hole overlap, leading to a 15-fold increase of the Huang-Rhys factor from 0.005 without Sb to 0.076 for a maximum local Sb content of 20%. The localization energy of the electrons at 5 K is reduced from 15 meV without Sb to 6 meV, while the hole localization increases from 18

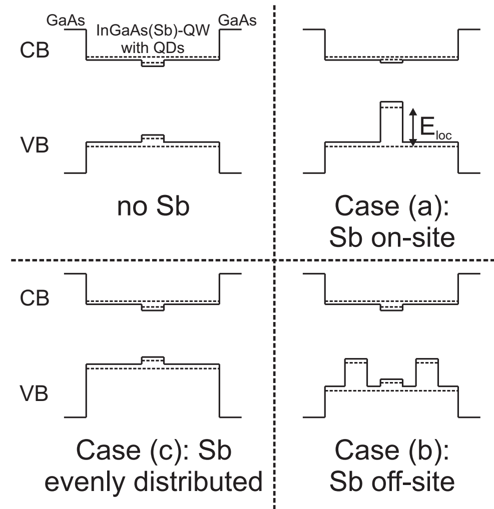


FIG. 3. Schematic band alignment for the different cases of Sb distribution; dotted lines indicate the energy levels of the quantum well and the embedded quantum dots.

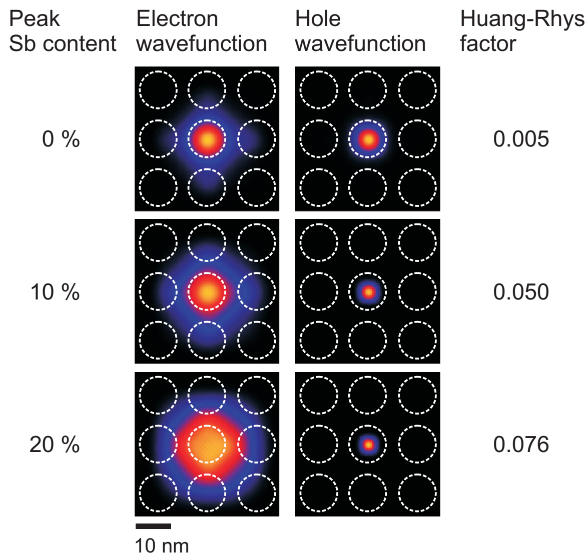


FIG. 4. (Color online) Electron and hole wave functions and Huang-Rhys factors as a function of Sb content for the case of Fig. 1(b) left (dashed white circles mark QDs defined by In-rich regions).

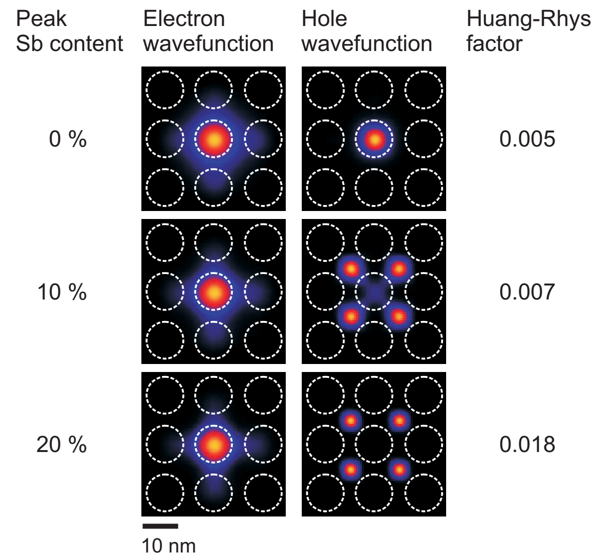


FIG. 6. (Color online) Electron and hole wave functions and Huang-Rhys factors as a function of Sb content for the case of Fig. 1(b) right (dashed white circles mark QDs defined by In-rich regions).

to 154 meV. An even distribution of the Sb throughout the SML stack as in case (b) only leads to a slightly stronger delocalization of the hole wave function (Fig. 5), resulting in a better overlap and consequently a smaller Huang-Rhys factor. Case (c), where the Sb is incorporated in between the QDs, leads to a localization of the hole wave function at the Sb-rich regions (Fig. 6), leading to a strong delocalization from the QDs and a Huang-Rhys factor increased to 0.018 for 20% Sb content due to the reduced overlap. In this case, the localization energy of the electron decreases from 15 to 13 meV, while the hole localization energy increases from 18 to 114 meV. This case yields the lowest overall strain in the system.

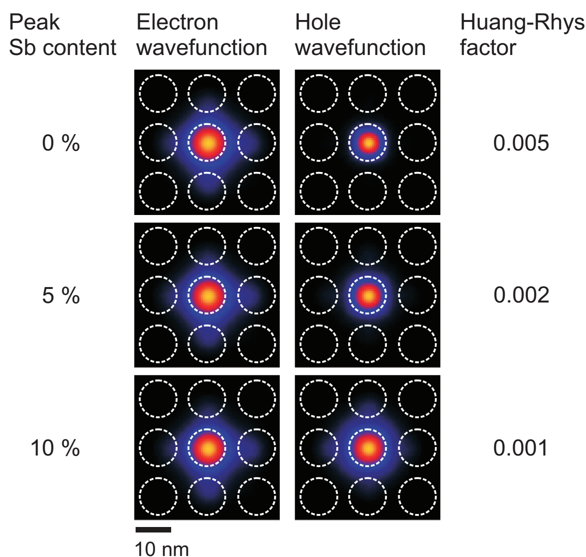


FIG. 5. (Color online) Electron and hole wave functions and Huang-Rhys factors for the case of even distribution of Sb throughout the SML stack dependent on the maximum Sb content (dashed white circles mark QDs defined by In-rich regions).

## III. EXPERIMENT

All samples are grown in a horizontal MOVPE reactor at 100 mbar pressure. After deoxidation of the GaAs(001) substrates and buffer layer growth, the structure containing the SML stacks was grown. The SML stacks were grown at a temperature of 520 °C with a V/III ratio of about 2 for both InAs and GaAs, using trimethylgallium, trimethylindium, and tertiarybutylarsine. The nominal thicknesses in the SML stack are 0.44 ML for InAs and 3.22 ML for GaAs, calibrated using a XRD structure grown without Sb (see Sec. IV). For samples containing Sb, a dedicated amount of Sb was supplied to the GaAs surface prior to each InAs SML growth using triethylantimony (TESb) as a precursor at a rate of 8.6 $\mu$mol/min, while all other sources were disabled. Sb flushes of up to 96 s were applied, corresponding to up to 13.8 $\mu$mol TESb supply (subsequently referred to as Sb flush). The basic SML layer structure is shown in Fig. 7.

The actual sample structures for the various investigations are given in the respective sections.

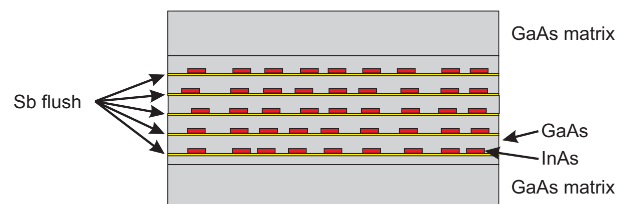


FIG. 7. (Color online) Basic layer arrangement (shown here for a 5 × SML stack).

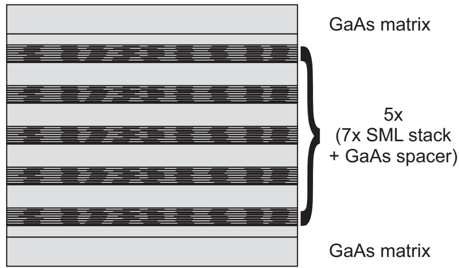


FIG. 8. Sample structure for investigations with XRD and HAADF-STEM.

## IV. STRUCTURAL PROPERTIES

### A. XRD and STEM investigations

The incorporation of Sb into the SML stack and its influence on the growth rates of InAs and GaAs is studied by investigating fivefold superlattices consisting of 7 × InAs(Sb)/GaAs SML stacks separated by GaAs spacers (see Fig. 8 ) with XRD. The measured spectra are then fitted assuming an InGaAsSb/GaAs superlattice, yielding the total thickness of the GaAs spacers and of the SML stacks as well as the average composition.

As shown in Fig. 9 the superlattice satellite reflections are well reproduced up to the third order for each structure, indicating the absence of long-range lateral composition fluctuations, even with the addition of Sb.

For an SML stack grown without an Sb flush the total thickness is determined to be 7.3 nm and the average In content to be $x_{\text{In}} = 0.128$. This corresponds to a thickness of 0.44 monolayers (MLs) InAs grown at 0.031 ML/s for each SML, which are separated by 3.22 MLs GaAs grown at 0.32 ML/s. For Sb supplies of 6.9 and 13.8 $\mu$mol, respectively, a good fit is found by assuming a 3.5 nm $In_{0.2}Ga_{0.8}As_{0.98}Sb_{0.02}$ and a 4.1 nm $In_{0.21}Ga_{0.79}As_{0.98}Sb_{0.02}$ quantum film. From this follows an increase of the total In + Sb amount by about 9%. Even for a low Sb supply of 1.7 $\mu$mol the In + Sb content is already increased by 8%. SML stacks grown with Sb flush are significantly thinner than without Sb flush. This reduction can be assigned to a reduced growth rate under Sb supply. By analyzing the average InAs and GaAs content of the SML stacks, a reduction of the GaAs growth rate by a factor of 2 is found in the SML stacks. Likewise, the growth rate of the GaAs spacers between the SML stacks is also affected. Here the thickness is reduced from 7.3 nm without Sb in the SML stack to 5.65 and 5.2 nm for 9.6 and 13.8 $\mu$mol Sb flush, respectively (see Fig. 9).

In contrast, the InAs growth rate is only reduced by about 10%. Sb is known to act as a reactive surfactant, taking the site of As atoms. The growth rate is therefore presumed to be governed by the rate of the As-for-Sb exchange process. Since such exchange increases the surface energy as compared to a Sb-terminated surface [30], the growth rate is limited and results in a stronger decrease for the ten times higher growth rate of GaAs compared to the lower InAs growth rate.

Similar 7 × InAs(Sb)/GaAs SML stacks were also investigated with a high-angle angular dark-field (HAADF) STEM with probe $C_s$ corrector and 300 kV electron beam acceleration voltage (see Fig. 9 insets). Here sharp interfaces to the adjacent GaAs matrix material can be seen in the images. In case of SML stacks with either 6.9 or 13.8 $\mu$mol Sb supply, no individual InAs sheets or In-rich clusters can be resolved due to the significantly thinner GaAs spacers.

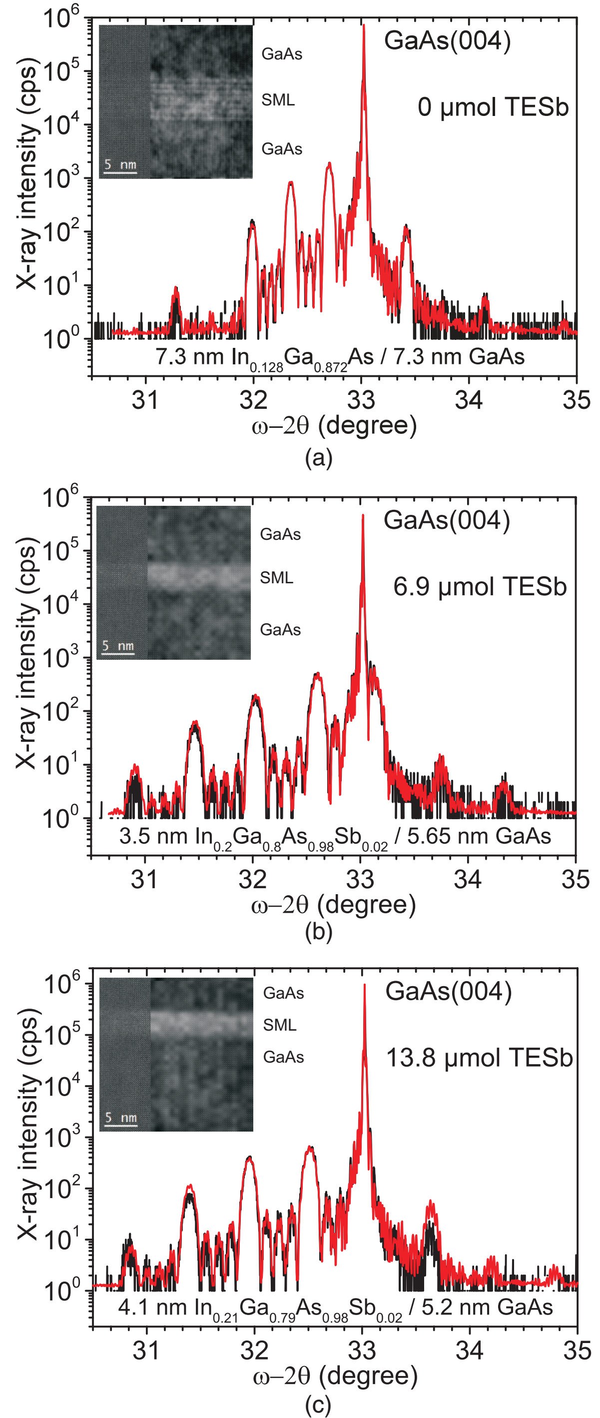


FIG. 9. (Color online) XRD spectra of fivefold superlattices containing 7 × InAs(Sb)/GaAs SML stacks grown with (a) 0 $\mu$mol, (b) 6.9 $\mu$mol, and (c) 13.8 $\mu$mol TESb. Rocking curve simulations are shown as red lines. Insets show HAADF-STEM images (left part: raw data, right part: filtered data) of single 7 × InAs(Sb)/GaAs SML stacks with the same nominal amount of Sb.

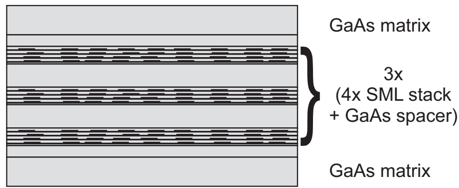


FIG. 10. Sample structure for investigation with XSTM.

### B. XSTM investigations

A detailed investigation of the positions of the individual atoms was performed by XSTM. Empty-state XSTM images at a threefold superlattice with 4 × InAs(Sb)/GaAs SML stacks, GaAs spacers, and an Sb supply of 13.8 $\mu$mol per growth cycle (see Fig. 10) show In-rich agglomerations of about 3.4 nm width and a density of about $2 \times 10^{12}$ cm$^{-2}$ [see Fig. 11(a)]. In comparison, SMLs grown without Sb show larger widths of about 5 nm, but about the same areal density [12]. An analysis of the variation of the local lattice constant (not shown here)

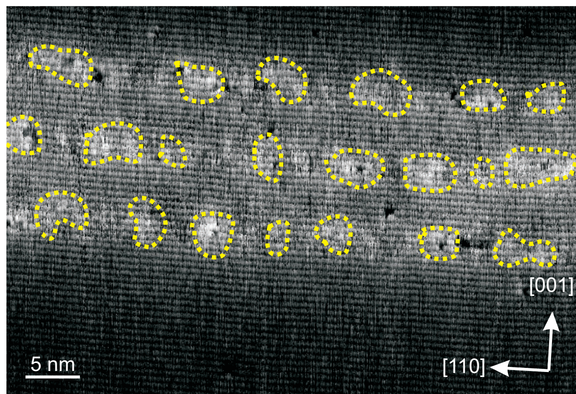


(a)

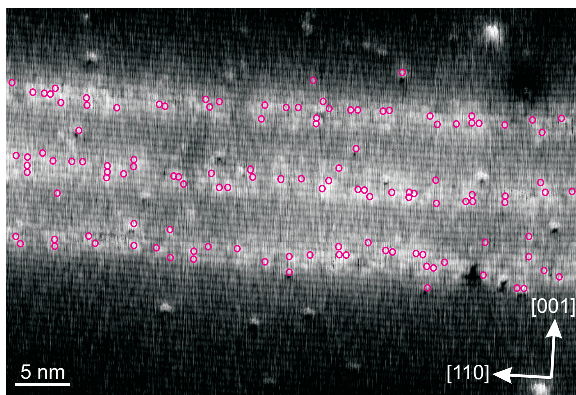


(b)

FIG. 11. (Color online) XSTM images of a threefold 4 × SML stack. (a) Empty-state image taken at a sample voltage of +2.4 V and a tunneling current of 40 pA, showing the In-rich regions (yellow dotted lines) in the SML stack. (b) Filled-state image taken at a sample voltage of −1.8 V and a tunneling current of 40 pA, emphasizing single Sb atoms, marked as (pink) solid circles. The images are not taken at exactly the same position of the sample, therefore no information concerning the relative positions of the In and Sb atoms can be deduced.

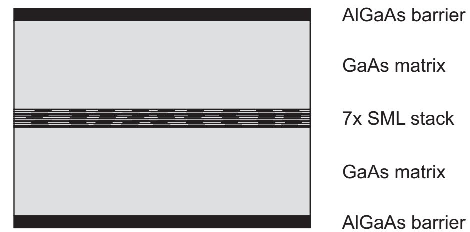


FIG. 12. Sample structure for investigation with PL.

shows that the segregation coefficient is $0.68 \pm 0.05$, which is not significantly smaller as compared to $0.75 \pm 0.07$ without Sb supply [11,12].

Filled-state XSTM images yielding a high contrast of the group-V sublattice [see Fig. 11(b)] show that the Sb atoms exhibit a slight clustering tendency which refutes case (b) of the Sb distribution introduced in Sec. II, where the Sb atoms are evenly distributed throughout the SML stack. The Sb atoms appear brighter than the As atoms in filled-state XSTM images because of their larger size, which results in a stronger surface buckling and therewith a stronger protrusion of the filled Sb dangling bonds responsible for the tunneling current [31]. Unfortunately, no measurements correlating the location of the Sb atoms with respect to the In atoms could be performed yet, leaving cases (a) and (c) open.

## V. OPTICAL PROPERTIES

For PL studies under cw excitation, single 7 × SML stacks with differing amounts of Sb supply are embedded into a 300 nm GaAs matrix, clad by lower and upper AlGaAs diffusion barriers (see Fig. 12).

Figure 13(a) shows PL spectra taken at 10 K. Even for the lowest amount of Sb supply (0.4 $\mu$mol TESb), a redshift of the peak energy from 1.400 to 1.377 eV and an increase of the FWHM is observed [see Fig. 13(b)]. With further increasing Sb flush the peak energy shifts monotonously towards 1.300 eV and the FWHM increases from 3.4 meV without Sb to 15.7 meV with 13.8 $\mu$mol Sb supply. As mentioned before, both thickness reduction as well as increased In + Sb content of the SML are already established at a supply of only 1.7 $\mu$mol TESb. Furthermore, the thickness and In + Sb content change only gradually for higher amounts of Sb supply. Hence, it is reasonable to assign the observed redshift to enhanced local potential fluctuations.

The addition of Sb to the growth sequence results in a reduction of the integrated PL intensity. The minimal ratio with respect to samples grown without Sb is 0.45. Since no decrease of the integrated PL intensity by an order of magnitude or more is observed, the SML stacks still exhibit a type-I band alignment. This would not be the case if the Sb is located in between the In-rich agglomerations, as described in case (c) of the simulation. Therefore, case (a) is the most likely one, in which the Sb is located at the In-rich agglomerations, which is not the state of lowest strain energy. A possible explanation is that the relaxation of a system into its lowest strain state is a slow process. Furthermore, the surface energies play an additional role during growth. Since the growth times are in the order of tens of seconds, it is possible that

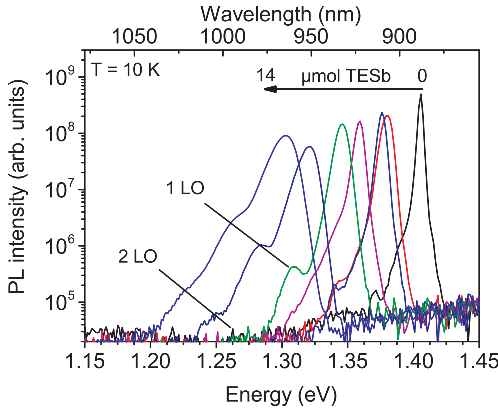


(a)

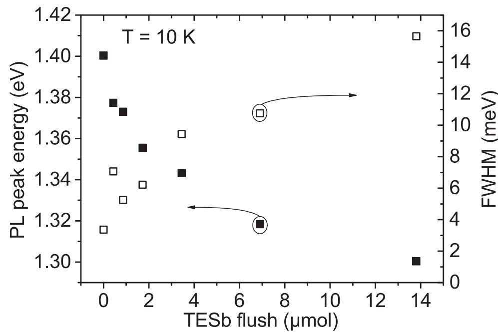


(b)

FIG. 13. (Color online) Low temperature PL measurements of single 7 × InAs(Sb)/GaAs SML stacks with increasing Sb supply. (a) PL spectra. (b) Shift of peak energy (filled squares) and FWHM (open squares) with increasing Sb flush.

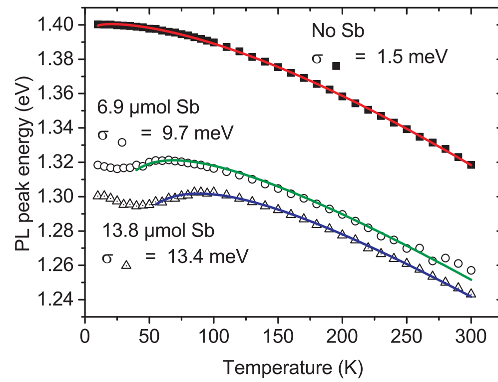


(a)

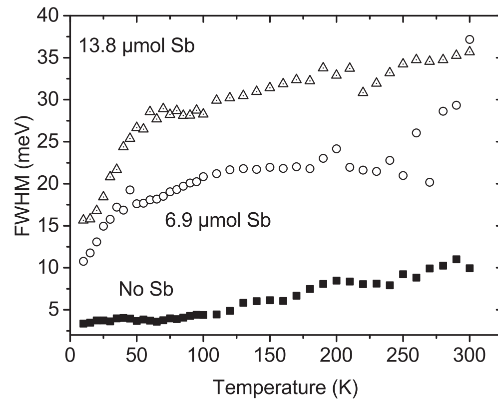


(b)

FIG. 14. (Color online) (a) Peak energies with fits (solid lines) for the potential fluctuations and (b) FWHM of temperature-dependent PL for 7 × SML stacks with no Sb (squares), 6.9 $\mu$mol Sb (circles), and 13.8 $\mu$mol (triangles).

there is insufficient time for a complete structural relaxation process.

Recording the temperature-dependent peak energies and values for the FWHM of the intensity distribution, as shown in Fig. 14 for samples with 0, 6.9, and 13.8 $\mu$mol Sb flush, reveals the development of an S shape as well as a significant increase in the FWHM with temperature. This behavior is characteristic for charge-carrier transfer between strongly and weakly localized states [32–34]. The magnitude and onset temperature of this carrier redistribution increases with the nominal Sb supply during growth. This result corresponds to the calculations of the band lineups shown in Sec. II, for which the localization of the holes increases with the Sb incorporation. For the structure without Sb flush, the temperature shift of the peak energy position can easily be explained as induced by band gap shrinkage [35]. For the structures with Sb supply a broadening term $\frac{\sigma^2}{k_B}T$ ($\sigma$ is a standard deviation from average $E_{\text{gap}}$, $k_B$ is the Boltzmann constant, and $T$ is temperature) needs to be added to the Varshni dependence of the band gap energy, resulting in an estimate to the magnitude of potential fluctuations within the layers containing Sb [36]. As shown in Fig. 14(a), the potential fluctuations increase from 1.5 meV for the sample without Sb to 9.7 and 13.4 meV for the samples with 6.9 and 13.8 $\mu$mol TESb, respectively. Close to room temperature, the thermally induced band gap reduction dominates the peak energy shift.

Using band lineups as proposed by Van de Walle [37] and interpolating the relevant alloy parameters from those of the constituent binary materials by using the compositions and thicknesses acquired from the XRD simulations (see Sec. IV A) the transition energies at $T = 0$ K can be obtained from single-particle 1D-Schrödinger equations. For 7.3 nm $In_{0.128}Ga_{0.872}As$ we find a ground state transition of 1.42 eV, for 3.5 nm $In_{0.2}Ga_{0.8}As_{0.98}Sb_{0.02}$ a transition energy of 1.39 eV, and for 4.1 nm $In_{0.21}Ga_{0.79}As_{0.98}Sb_{0.02}$ a transition energy of 1.37 eV. Taking into account band gap reduction, at room temperature reasonable agreement with room-temperature PL data is achieved for the sample without Sb. The emission of the samples with Sb is significantly redshifted as compared to the simulation (see Fig. 15).

Figure 16 shows spatially resolved CL spectra of SML stacks grown either without or with 1.7 $\mu$mol Sb flush recorded through small (∼100–200 nm diameter) apertures in an electron-transparent metal film. SML stack heights are adjusted to yield approximately similar peak energies at $T = 10$ K. Integral PL spectra on a semilogarithmic scale are additionally given as reference in Fig. 18. Individual CL spectra of the SML stack grown without Sb supply do not exhibit any spatial variation nor single excitonic emission lines. In contrast, for samples with Sb flush narrow individual emission lines are resolved within the integral luminescence.

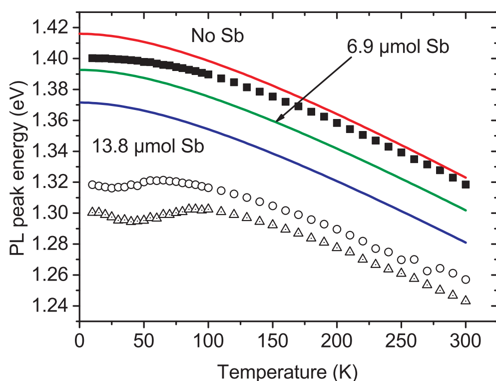


FIG. 15. (Color online) Peak energies of temperature-dependent PL with simulation (solid lines) of quantum wells showing band gap shrinkage.

This provides direct evidence for an enhanced localization of charge carriers as predicted by the eight-band $k \cdot p$ simulations of case (a) and proves that by adding Sb to the SML growth sequence, zero dimensional states develop [38]. As shown in Fig. 16 the relative intensity of the longitudinal optical (LO) phonon peak increases in the presence of Sb. From a sample series of $7\times$ SML stacks with varying amounts of Sb supply an increase of the Huang-Rhys factor ($I \sim S^n e^{-S}/n!$, with $I$ and $n$ being the intensity and order of the LO phonon peak, and

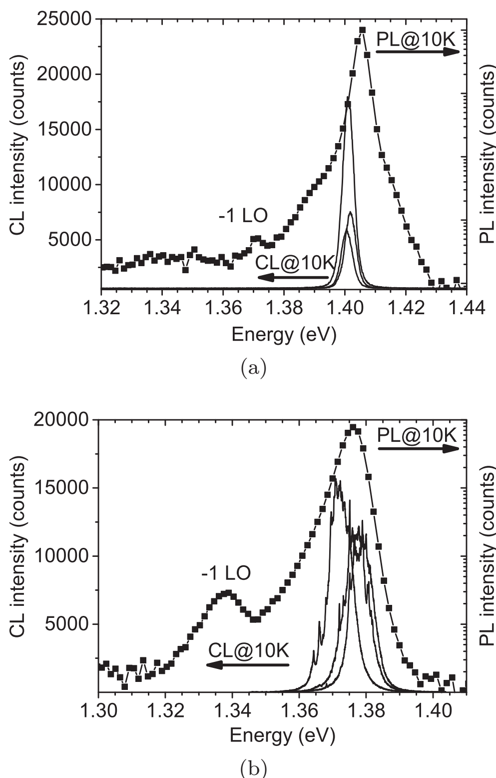


FIG. 16. Spatially resolved CL spectra (solid lines) of (a) $7\times$ InAs/GaAs SML stacks grown without Sb, and (b) $12\times$ InAs(Sb)/GaAs SML with 1.7 $\mu$mol Sb flush. The different spectra correspond to the varying positions on the sample. For comparison, integral PL data (solid lines + squares) is plotted.

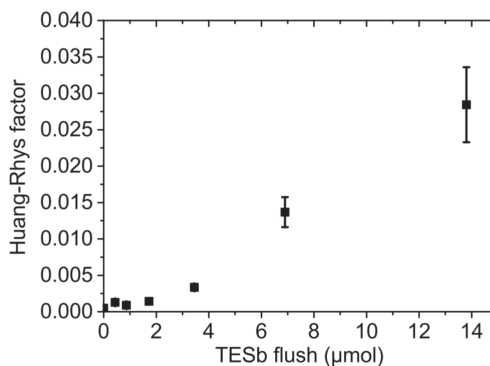


FIG. 17. Huang-Rhys factor for $7\times$ InAs/GaAs SML stacks with different amounts of Sb supply, the large error for the Huang-Rhys factor at 13.8 $\mu$mol Sb is due to the large error in the amplitude determination [see Fig. 13(a)].

$S$ being the Huang-Rhys factor) [29] from $0.0005 \pm 0.0001$ to $0.0284 \pm 0.0052$ can be observed (see Fig. 17).

This indicates an enhanced dipole moment due to the localization of charge carriers and coincides with case (a) from the eight-band $k \cdot p$ simulations shown in Sec. II. For (InGa)As quantum dots Heitz *et al.* have theoretically and experimentally determined a Huang-Rhys factor of about 0.015 [39,40] which also agrees with the values obtained in this work. The energetic difference between the 0 LO phonon and the $-1$ LO phonon peak is around 34 meV, being close to the value 35.3 meV of the GaAs optical phonon [41].

The emission peak energy of a SML stack can be adjusted independently of the Sb flush by properly choosing the quantity of InAs sheets and thickness of GaAs spacer layers in between them. An example is illustrated in Fig. 18 where SML stacks grown with different Sb flushes were adjusted to about the same wavelength of around 970 nm ($h\nu = 1.28$ eV). With increasing Sb flush the FWHM of the SML luminescence is broadened from 11.4 nm (0 $\mu$mol TESb) to 46.3 nm (13.8 $\mu$mol TESb). This feature allows for designing the electronic properties of an active medium to specific target applications such as gain bandwidth or maximum peak gain. It is noteworthy that QD emission around 900 nm wavelength using InAs/GaAs SML stacks is realized. For InAs/GaAs Stranski-Krastanov QDs this wavelength region around and

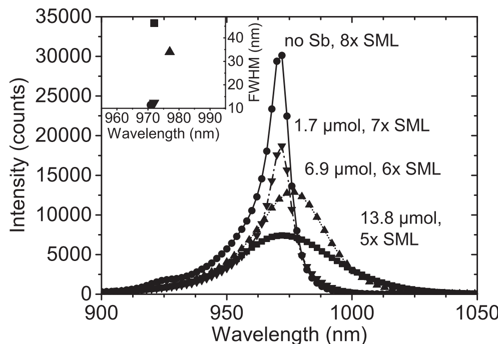


FIG. 18. PL at 300 K showing increased FWHM of SML stacks with increasing amount of Sb prior to InAs deposition. The inset shows the corresponding FWHMs.

below 900 nm is not easy to access due to the minimum layer thickness required for the 2D/3D growth mode transition. Even shorter wavelengths may be achieved by utilizing AlGaAs as spacer material between the InAs sheets [42].

## VI. CONCLUSION

The influence of Sb flushes on the electronic and optical properties of InAs/GaAs submonolayer stacks has been theoretically and experimentally investigated. Eight-band $k \cdot p$ simulations predict a redshift of the emission energy for different cases of Sb incorporation in or beside In-rich regions as well as hole localization at the Sb-rich regions. All experimental results show an incorporation of the Sb into the QDs formed by In-rich regions in the SML stacks. Sb further affects the growth rate, resulting in an increased In + Sb content of the submonolayer, but does not lead to a change of growth mode. XSTM measurements show smaller In-rich agglomerations as compared to SML stacks without Sb and also a slight clustering of Sb atoms. An enhanced carrier localization is evidenced by a sigmoidal temperature dependence of the peak energy position, an increased FWHM of the luminescence intensity distribution, and an increased Huang-Rhys factor at low temperatures. In addition, individual sharp emission lines are found in spatially resolved CL spectra also at short wavelengths, which are otherwise not accessible with Stranski-Krastanow QDs. SML stacks with different degrees of localization can be realized for the same target wavelength by simultaneously adjusting the SML stack height and Sb supply.

Detailed investigations of the polarization properties and the differential gain as well as the modulation frequency of the SMLs with Sb will be reported elsewhere.

## ACKNOWLEDGMENTS

The authors thank J. Schuppang for assistance during XSTM measurements, M. Dähne for fruitful discussion of the manuscript, and the CRC 787 of the Deutsche Forschungsgemeinschaft for financial support. M. Weyland acknowledges the support of the Australian Research Council (ARC) under LE0454166 for equipment funding.

[1] M. Asada, Y. Miyamoto, and Y. Suematsu, IEEE J. Quantum Electron. **22**, 1915 (1986).
[2] N. Kirstaedter, O. G. Schmidt, N. N. Ledentsov, D. Bimberg, V. M. Ustinov, A. Y. Egorov, A. E. Zhukov, M. V. Maximov, P. S. Kopev, and Z. I. Alferov, Appl. Phys. Lett. **69**, 1226 (1996).
[3] D. Bimberg, N. Kirstaedter, N. N. Ledentsov, Z. I. Alferov, P. S. Kop'ev, and V. M. Ustinov, IEEE J. Sel. Top. Quantum Electron. **3**, 196 (1997).
[4] J. H. Blokland, M. Bozkurt, J. M. Ulloa, D. Reuter, A. D. Wieck, P. M. Koenraad, P. C. M. Christianen, and J. C. Maan, Appl. Phys. Lett. **94**, 023107 (2009).
[5] D. M. Bruls, J. W. A. M. Vugs, P. M. Koenraad, H. W. M. Salemink, J. H. Wolter, M. Hopkinson, M. S. Skolnick, F. Long, and S. P. A. Gill, Appl. Phys. Lett. **81**, 1708 (2002).
[6] H. Eisele, O. Flebbe, T. Kalka, C. Preinesberger, F. Heinrichsdorff, A. Krost, D. Bimberg, and M. Dähne-Prietsch, Appl. Phys. Lett. **75**, 106 (1999).
[7] S. Gaan, G. He, R. M. Feenstra, J. Walker, and E. Towe, J. Appl. Phys. **108**, 114315 (2010).
[8] B. Lita, R. S. Goldman, J. D. Phillips, and P. K. Bhattacharya, Appl. Phys. Lett. **74**, 2824 (1999).
[9] Q. Xie, A. Madhukar, P. Chen, and N. P. Kabayashi, Appl. Phys. Lett. **75**, 2542 (1995).
[10] S. Ruvimov, P. Werner, K. Scheerschmidt, U. Gösele, J. Heydenreich, U. Richter, N. N. Ledentsov, M. Grundmann, D. Bimberg, V. M. Ustinov, A. Y. Egorov, P. S. Kop'ev, and Z. I. Alferov, Phys. Rev. B **51**, 14766 (1995).
[11] A. Lenz, H. Eisele, J. Becker, L. Ivanova, E. Lenz, F. Luckert, K. Pötschke, A. Strittmatter, U. W. Pohl, D. Bimberg, and M. Dähne, Appl. Phys. Express **3**, 105602 (2010).
[12] A. Lenz, H. Eisele, J. Becker, J.-H. Schulze, T. D. Germann, F. Luckert, K. Pötschke, E. Lenz, L. Ivanova, A. Strittmatter, D. Bimberg, U. W. Pohl, and M. Dähne, J. Vac. Sci. Technol. B **29**, 04D104 (2011).
[13] I. L. Krestnikov, N. N. Ledentsov, A. Hoffmann, and D. Bimberg, Phys. Status Solidi (a) **183**, 207 (2001).
[14] V. A. Shchukin, D. Bimberg, V. G. Malyshkin, and N. N. Ledentsov, Phys. Rev. B **57**, 12262 (1998).
[15] Z. Xu, D. Birkedal, J. Hvam, Z. Zhao, Y. Liu, K. Yang, A. Kanjilal, and J. Sadowski, Appl. Phys. Lett. **82**, 3859 (2003).
[16] Z. Xu, K. Leosson, D. Birkedal, V. Lyssenko, J. Hvam, and J. Sadowski, Nanotechnology **14**, 1259 (2003).
[17] Z. Xu, Y. Zhang, J. Hvam, J. Xu, X. Chen, and W. Lu, Appl. Phys. Lett. **89**, 013113 (2006).
[18] Z. Xu, D. Birkedal, M. Juhl, and J. Hvam, Appl. Phys. Lett. **85**, 3259 (2004).
[19] S. S. Mikhrin, A. E. Zhukov, A. R. Kovsh, N. A. Maleev, V. M. Ustinov, Y. M. Shernyakov, I. P. Soshnikov, D. A. Livshits, I. S. Tarasov, D. A. Bedarev, B. V. Volovik, M. V. Maximov, A. F. Tsatsul'nikov, N. N. Ledentsov, P. S. Kop'ev, D. Bimberg, and Z. I. Alferov, Semicond. Sci. Technol. **15**, 1061 (2000).
[20] Y. Arakawa and A. Yariv, IEEE J. Quantum Electron. **22**, 1887 (1986).
[21] D. Bimberg, M. Grundmann, and N. N. Ledentsov, *Quantum Dot Heterostructures* (Wiley, New York, 1999).
[22] A. E. Zhukov, A. R. Kovsh, S. S. Mikhrin, N. A. Maleev, V. M. Ustinov, D. A. Livshits, I. S. Tarasov, D. A. Bedarev, M. V. Maximov, A. F. Tsatsul'nikov, I. P. Soshnikov, P. S. Kop'ev, Z. I. Alferov, N. N. Ledentsov, and D. Bimberg, Electron. Lett. **35**, 1845 (1999).
[23] T. D. Germann, A. Strittmatter, J. Pohl, U. W. Pohl, D. Bimberg, J. Rautiainen, M. Guina, and O. G. Okhotnikov, Appl. Phys. Lett. **92**, 101123 (2008).
[24] F. Hopfer, A. Mutig, M. Kuntz, G. Fiol, D. Bimberg, N. N. Ledentsov, V. A. Shchukin, S. S. Mikhrin, D. L. Livshits, I. L. Krestnikov, A. R. Kovsh, N. D. Zakharov, and P. Werner, Appl. Phys. Lett. **89**, 141106 (2006).

[25] N. N. Ledentsov, D. Bimberg, F. Hopfer, A. Mutig, V. A. Shchukin, A. V. Savel'ev, G. Fiol, E. Stock, H. Eisele, M. Dähne, D. Gerthsen, U. Fischer, D. Litvinov, A. Rosenauer, S. S. Mikhrin, A. R. Kovsh, N. D. Zakharov, and P. Werner, Nanoscale Res. Lett. **2**, 417 (2007).
[26] T. Kita, N. Tamura, O. Wada, M. Sugawara, Y. Nakata, H. Ebe, and Y. Arakawa, Appl. Phys. Lett. **88**, 211106 (2006).
[27] P. Ridha, L. H. Li, M. Mexis, P. Smowton, J. Andrzejeweski, G. Sek, J. Misiewicz, E. P. O'Reilly, G. Patriarche, and A. Fiore, IEEE J. Quantum Electron. **46**, 197 (2010).
[28] O. Stier, M. Grundmann, and D. Bimberg, Phys. Rev. B **59**, 5688 (1999).
[29] K. Huang and A. Rhys, Proc. R. Soc. London Ser. A **204**, 406 (1950).
[30] Y. Q. Wang, Z. L. Wang, T. Brown, A. Brown, and G. May, J. Crystal Growth **242**, 5 (2002).
[31] R. Timm, A. Lenz, H. Eisele, L. Ivanova, M. Dähne, G. Balakrishnan, D. L. Huffaker, I. Farrer, and D. A. Ritchie, J. Vac. Sci. Technol. B **26**, 1492 (2008).
[32] R. Heitz, I. Mukhametzhanov, A. Hoffmann, and D. Bimberg, J. Electron. Mater. **28**, 520 (1999).
[33] Q. Li, S. J. Xu, M. H. Xie, and S. Y. Tong, J. Phys.: Condens. Matter **17**, 4853 (2005).
[34] L. Brusaferri, S. Sanguinetti, E. Grilli, M. Guzzi, A. Bignazzi, F. Bogani, L. Carraresi, M. Colocci, A. Bosacchi, P. Frigeri, and S. Franchi, Appl. Phys. Lett. **69**, 3354 (1996).
[35] Y. P. Varshni, Physica **34**, 149 (1967).
[36] J. Christen and D. Bimberg, Phys. Rev. B **42**, 7213 (1990).
[37] C. Van de Walle, Phys. Rev. B **39**, 1871 (1989).
[38] M. Grundmann, J. Christen, N. N. Ledentsov, J. Böhrer, D. Bimberg, S. S. Ruvimov, P. Werner, U. Richter, U. Gösele, J. Heydenreich, V. M. Ustinov, A. Y. Egorov, A. E. Zhukov, P. S. Kop'ev, and Z. I. Alferov, Phys. Rev. Lett. **74**, 4043 (1995).
[39] R. Heitz, I. Mukhametzhanov, O. Stier, A. Madhukar, and D. Bimberg, Phys. Rev. Lett. **83**, 4654 (1999).
[40] R. Heitz, H. Born, A. Hoffmann, D. Bimberg, I. Mukhametzhanov, and A. Madhukar, Appl. Phys. Lett. **77**, 3746 (2000).
[41] S. Adachi, *Properties of Group-IV, III-V and II-VI Semiconductors* (Wiley, New York, 2005).
[42] L. Yu, D. Jung, S. Law, J. Shen, J. J. Cha, M. L. Lee, and D. Wassermann, Appl. Phys. Lett. **105**, 081103 (2014).